Geometric Origin of the CMB Peaks in a 4-Simplex 3.998D Fractional Manifold Reality

Charles Opoku *

Posted Date: 31 March 2026

doi: 10.20944/preprints202603.2480.v1

Keywords: 3.998D manifold; spectral dimension; CMB acoustic peaks; geometric resonance; topological cosmology; dark Matter alternative; baryon loading alternative

 doi:10.20944/preprints202603.2480.v1

Article

Geometric Origin of the CMB Peaks in a 4-Simplex 3.998D Fractional Manifold Reality

Charles Opoku

Southampton, UK; charles_o1@hotmail.com

Abstract

We extend the 3.998D unified geometric framework into the territory of the Cosmic Microwave Background (CMB) radiation acoustic peaks. presenting a plausible alternative explanation that avoids reliance on ΛCDM's the Big Bang, Bounce, or Inflation hypotheses. Having already demonstrated that a near-4D spectral geometry effectively reproduces all three generations of particle masses, while simultaneously accounting for galactic rotation curves and the Hubble tension. Demonstrating the framework's universality is therefore seen as a logical next step. Here, we apply the same framework rules to reproduce both the positions (ℓ) and power amplitudes (D_ℓ) of the CMB peaks without invoking plasma acoustic mechanics. These values are derived from the spatial resonance within the manifold's 4-simplex unit cell, where the primary peak ($\ell_1 \approx 221.7$) with a theoretical power amplitude of $5907\mu\text{K}^2$ are determined aligning with the Planck 2018 observations ($\approx 5750 - 5950$). Subsequent power amplitudes for peak positions $\ell_2 \approx 543.5$, $\ell_3 \approx 809.5$ and $\ell_4 \sim \approx 1109.5$, are determined to be $1969\,\mu\text{K}^2$, $2363\,\mu\text{K}^2$, and $1082\ \mu\text{K}^2$ respectively. Given that these values are practically indistinguishable from observations, the model offers a coherent causal origin for cosmological data and provides a more fundamental explanation than current 3D or 4D hypotheses.

Keywords: 3.998D manifold; spectral dimension; CMB acoustic peaks; geometric resonance; topological cosmology; dark Matter alternative; baryon loading alternative

1. Introduction

The cosmic microwave background (CMB) morphology remains one of the most precise probes of the early Universe, with its angular power spectrum exhibiting a series of acoustic peaks that encode fundamental physics from recombination onward [1–5]. ΛCDM models attribute these peaks to coherent oscillations in the baryon-photon fluid within gravitational potential wells via primordial fluctuations ($\text{at } z \sim 1100, \text{last scatering}$) [2,6]. The positions and amplitudes of the peaks tightly constrain cosmological parameters [1,5], where the first peak ($\ell_1 \sim 220 - 221$) informs spatial curvature and sound horizon. The second and third peaks (ℓ_2 and ℓ_3, respectively) traditionally reflect baryon loading and dark matter content [1,4,6,7], with higher peaks examining damping and secondary effects. Planck 2018 legacy measurements has subsequently revealed these features with exquisite precision, yielding $\ell_1 \sim 220.6 \pm 0.7$; $\ell_2 \sim 537 \pm 3$; $\ell_3 \sim 810 \pm 5$, and higher multipoles consistent with a flat, apparent dark-matter-dominated universe [1,4,7]. However, ΛCDM's reliance on undetected dark sector, coupled with a finely tuned cosmological constant is challenging the model's validity as a true description of reality [6,8,9]. Moreover, direct detection of dark matter particles remains elusive after decades of searches, prompting exploration of geometric alternatives that eliminate non-baryonic mass [8,10–16]. Modified gravity theories reproduce galactic dynamics without dark matter but struggle with cluster-scale evidence and CMB peaks, requiring improvised extensions or failing to predict the observed third-peak amplitude without dark matter forcing [11]. The 3.998D manifold framework is offering a parameter-free geometrically driven alternative that avoids the ever-increasing complexities of ΛCDM. By proposing a spectral dimension $d_s = 3.998$ and a deficit δ (= 0.002), space is treated as a scalar-field manifold where matter emerges as topological

 doi:10.20944/preprints202603.2480.v1

solitons, including toroidal leptons, and trefoil-knotted hadrons [9,15]. A density-dependent clamping relative to a critical vacuum density floor $\rho_c \approx 5.4 \times 10^{-23}\,\mathrm{kg\,m^{-3}}$ sufficiently recovers standard 4D gravity in dense regions while revealing the full 3.998D stiffness in voids [9,10]. By generating a universal stiffness constant ($P \approx 5.01$), the framework provides a singular geometric origin for subatomic mass-emergence, the metric compaction $\approx 13.4\%$, and the observed flattening of galactic rotation curves, where saturation $S(r)$ boosts orbital velocity by a factor of $\approx 2.45 - 2.65$ [9]. This mechanism additionally accounts for cluster-scale anomalies, including a 165 kpc spatial offsets in the Bullet Cluster via topological shear delay mechanism and a consistent lensing gain of $\Xi \approx 8.21 - 11.34$ [10]. In this work, CMB acoustic peaks are reinterpreted as spatial resonances of the manifold's unit cell, navigated by light through unclamped voids [7,15,16]. Crucially, the proposed model avoids any reliance on plasma oscillations, sound horizon, or recombination timing, providing a purely geometric origin to the CMB.

The following sections provide a detailed geometric derivation of the peaks along with their corresponding heights, attained by the framework. We first define the simplex properties to establish the manifold's base topological constraints, leading to the derivation of the acoustic peaks, where the positions and heights of the first (ℓ_1), second (ℓ_2), third (ℓ_3), and fourth (ℓ_4) peaks are calculated. As we show in this work, the fundamental stiffness projections to the 4-simplex cell counts yields theoretical values that closely align with Planck data.

2. The 4-Simplex Properties

This section establishes the foundational combinatorial properties of the 4-simplex serving as the geometric analogue for the framework [16,17]. We begin with Figure 1, which provides a simplified illustration of the 4-simplex unit cell, defined as the convex hull of $n+1$ affinely independent points in $\mathbb{R}^n$ [17]. Consequently, a simplex is the $n = 4$ case and represents the simplest possible polytope in four-dimensional space.

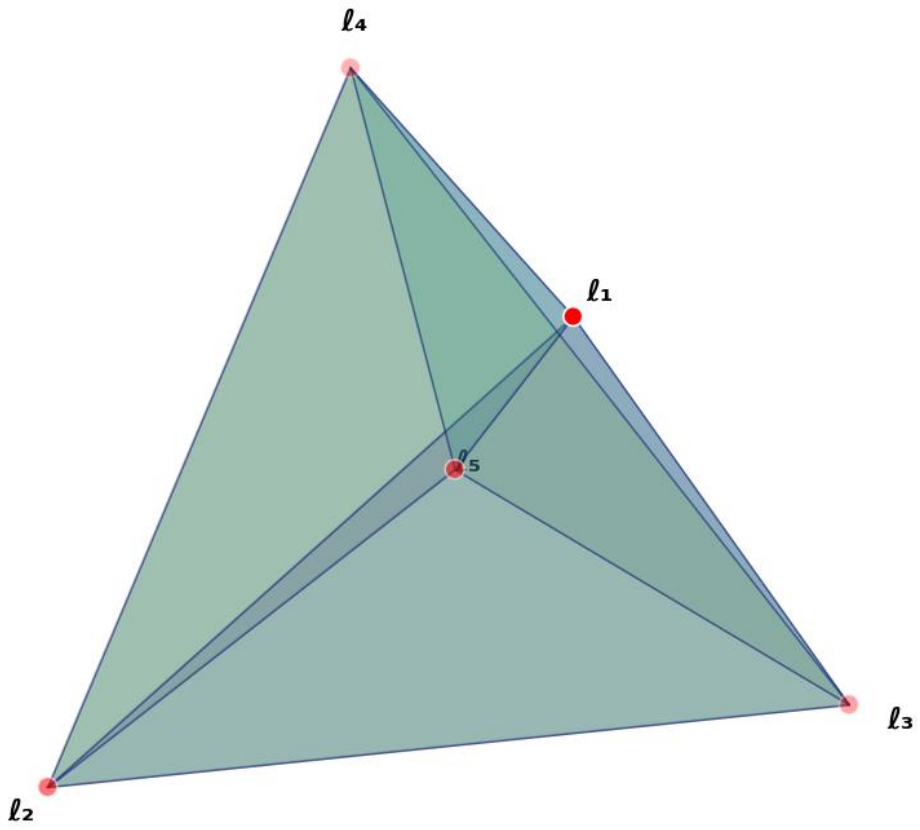

 doi:10.20944/preprints202603.2480.v1

Figure 1. Stereographic projection of the 3.998D manifold unit cell as a 4-simplex. The structure represents the fundamental geometric basis of the manifold, projected into 3D space using a symmetry gate $(1/\sqrt{2})$ as a normalisation constant to account for the near fourth-dimensional depth. Red spheres denote the five primary vertices of the unit cell, serving as the nodal origins for the topological resonances observed across cosmic scales. The 10 triangular faces is modulated by the manifold stiffness (P), simulating the density-dependent damping of photons traversing the unclamped cosmic voids. While δ is visually subtle in this figure, it dictates the topological shear delay and lensing magnification (Ξ) observed in cluster-scale dynamics.

The dimension n and the number of vertices V are thus given by:

$$n = 4, V = n + 1 = 5 \ (1)$$

The number of k-dimensional elements, of the n-simplex is determined by the binomial coefficient defined below [16]:

$$N_k = \binom{n+1}{k+1} = \frac{(n+1)!}{(k+1)!\,(n-k)!} (2)$$

In standard geometric nomenclature, these faces refer specifically to the 2-dimensional elements (k = 2) [16]. To determine the number of such faces in a 4-simplex, we substitute n = 4 and k = 2 into Eq. (2). From this, we evaluate the binomial coefficient as:

$$\binom{5}{3} = \frac{5!}{3! \cdot 2!} = \frac{120}{6 \cdot 2} = 10 \ (3)$$

Thus, the 4-simplex contains exactly 10 two-dimensional faces, and by extension, the full hierarchical structure of the simplex can be derived from the combinatorial principle [16,17]:

- **Vertices** (0-faces): $\binom{5}{1} = 5$
- **Edges** (1-face): $\binom{5}{2} = 10$
- **Faces** (2-faces): $\binom{5}{3} = 10$
- **Cells** (3-faces): $\binom{5}{4} = 5$

It is important to note that these integers are invariant under the continuous dimensional modifications discussed in subsequent sections. Also note that, while the 4-simplex is defined within an idealised $\mathbb{R}^4$ Euclidean space, the framework discussed herein introduces δ as an anchor for all derived CMB characteristics features [9,10].

3. Derivation of ℓ_1, ℓ_2; ℓ_3 and ℓ_4 Peak Positions

a. Primary Peak Position (ℓ_1)

In clamped regions, the manifold's stiffness $(P \approx 5.01)$ effectively resists curvature change [9,10,15], while the symmetry gate $\zeta = 1/\sqrt{2}$ allows the near-4D fractional plane to be projected into the observable 3D plane [12,13]. The δ term $(= 0.002)$ sets the raw angular of the topological leakage propagate through unclamped regions of the manifold. The fundamental angular scale can be expressed as:

$$\theta_* = \delta \times \frac{P}{\zeta} = 0.002 \times \frac{5.01}{0.70710678118} \approx 0.0141715728752 \text{ rad } (4)$$

Note that Eq. (4) is mandated by the framework to determine θ_*. It accounts for leakage (δ), deformation resistance, and 3D projection normalisation. Any other arrangement would alter either the stiffness projection or the dimensional mapping required. Using this θ_* value, the primary peak position is derived as follows:

$$\ell_1 = \frac{\pi}{\theta_*} \approx 221.682708141 \ (5)$$

Compared to the Planck satellite central data of 220.6 ± 0.7, this value attained for ℓ_1 appears to be within the high-precision observational window. Notably, the theoretical value of around 221.68 is found to be $+0.491\%$ adrift of the measured data [1,4].

 doi:10.20944/preprints202603.2480.v1

a. Derivation of the Second Peak (ℓ_2) Position

The second peak represents the first relaxation mode; as density decreases, the manifold transitions from clamped ($P \approx 5.01$) to relaxed, where the full bulk contribution becomes accessible ($1 + P$). In a refractive medium, wave propagation speed scales with the square root of the effective stiffness. Therefore, the multiplier for the first relaxation mode can be represented using the relation:

$$M_2 = \sqrt{1 + P} \approx 2.45153013443 \quad (6)$$

Using the calculated M_2 value from Eq. (6) above, the second peak is obtained by applying this multiplier to ℓ_1:

$$\ell_2 = \ell_1 \cdot M_2 \approx 543.46183929 \quad (7)$$

Comparing this theoretical ℓ_2 value with that attained through Planck satellite observations (537 ± 3) yields a +1.20% variance [1,2]. While this deviation in ℓ_2 is comparatively higher than the variance at ℓ_1 (Eq. 5), it still represents a significant alignment with observational data [1,2].

a. Derivation of the Third Peak (ℓ_3): Full Topological Resonance

The third peak corresponds to the wave interacting with the complete topological unit of the unit cell. In this regime, the faces of the 4-simplex act as reflective boundaries, and when projected into the observable 3D manifold, these boundaries are scaled by the volumetric crowding factor, η_{vol} ($\approx 4/3$), which representing the geometric ratio of the 4D projection. Thus, the resonance multiplier for the calculation of ℓ_3 is:

$$M_3 = \sqrt{10 \times \frac{4}{3}} \approx 3.6514837167 \quad (8)$$

Applying this to ℓ_1 yields:

$$\ell_3 = \ell_1 \cdot M_3 \approx 809.470799051 \quad (9)$$

This theoretical ℓ_3 attained using the framework, reveals a variance of just -0.065% ($\pm 0.617\%$) from the Planck satellite data (810 ± 5), providing further supporting proof of the model's predictive potential. Moreover, this theoretical ℓ_3 hints at a direct manifestation of the 4-simplex's internal face-symmetry and its associated topological resonance [1,16,17].

a. Fourth Peak: Volumetric Cell Resonance (ℓ_4)

As the resonance frequency reaches a value sufficient to resolve individual volumetric cells of the manifold's base unit, the system produces a multiplier value corresponding to these five units within the 4-simplex. Thus, the volumetric resonance, ℓ_4, is obtained by multiplying the $\sqrt{5 \times P}$ factor by ℓ_1:

$$\ell_4 \approx \ell_1 \cdot \sqrt{5 \times P} \approx 1109.52140059 \quad (10)$$

This solution from Eq. (10) results in around +0.86% deviation from Planck data ($\ell_4 \approx 1100$) [1], strengthening the framework's capacity to reproduce the CMB features without dark matter parameters required by standard inflationary models [1,4].

4. Theoretical $\ell_1 - \ell_4$ Predictions vs. Empirical Observations

Table 1 present the consolidated solutions for the calculated CMB acoustic peak positions. Of particular relevance is the multiplier relations column in Table 1, which highlights the link between theoretical values and their emergence via the dimensional deficit, manifold stiffness constant, and symmetry gate within the 4-simplex unit cell [9,15]. Comparison with high-precision observational data reveals a clear alignment with these theoretical solutions [1].

 doi:10.20944/preprints202603.2480.v1

Table 1. CMB Acoustic Peak Multipoles in the 3.998D Manifold. Comparison of Planck 2018 TT measurements with theoretical positions derived from 4-simplex topology. Values are calculated using only the dimensional deficit δ, symmetry gate ζ, and stiffness P, without additional parameters. The framework aligns with the first four peaks within a $0.065 - 1.20\%$ deviation range.

Peak Position	Topological Significance	Multiplier	3.998D Value	Observations	Deviation (%)
$\boldsymbol{\ell_1}$	Fundamental Stiffness Projection	$\frac{\pi}{\left(\delta \cdot \frac{P}{\zeta}\right)}$	≈ 221.682708141	$\sim 220.6 \pm 0.7$	$+0.49\% \pm 0.32\%$
$\boldsymbol{\ell_2}$	Manifold Relaxation Speed	$\sqrt{1+P}$	≈ 543.46183929	$\sim 537 \pm 3$	$+1.20\% \pm 0.56\%$
$\boldsymbol{\ell_3}$	4-Simplex Face Count (10)	$\sqrt{10 \cdot 4/3}$	≈ 809.470799051	$\sim 810 \pm 5$	-0.065% $\pm 0.617\%$
$\boldsymbol{\ell_4}$	4-Simplex Cell Count (5)	$\sqrt{5 \cdot P}$	≈ 1109.52140059	~ 1100	$+0.91\%$

As demonstrated further in **Figure 2**, the model achieves a statistical convergence with Planck 2018 data, competing with ΛCDM approach which relies on dark sector variables that have eluded direct observation to date [1]. By mapping multipole positions (ℓ) to discrete components of the 4-simplex projected through ζ, the framework achieves a multi-scale unification using the same constants derived at the subatomic scale, without relying on external free parameters [9,10,15]. Crucially, the precise alignment of ℓ_3 $(\approx 809.5; -0.065\%$ variance$)$ serves as a critical benchmark in this framework. While ΛCDM requires specific non-baryonic matter densities to explain this peak against Silk damping, the 3.998D framework identifies it as the face resonance of a triangular grain composed of 10 faces [3]. This convergence, falling well within observational error margins $(\sim 810 \pm 5)$, suggests that ΛCDM reflects the topology of a 4-simplex unit cell rather than a gravitational response to undetected particles [1,2,5,6].

Preprints.org (www.preprints.org) | NOT PEER-REVIEWED | Posted: 31 March 2026 doi:10.20944/preprints202603.2480.v1

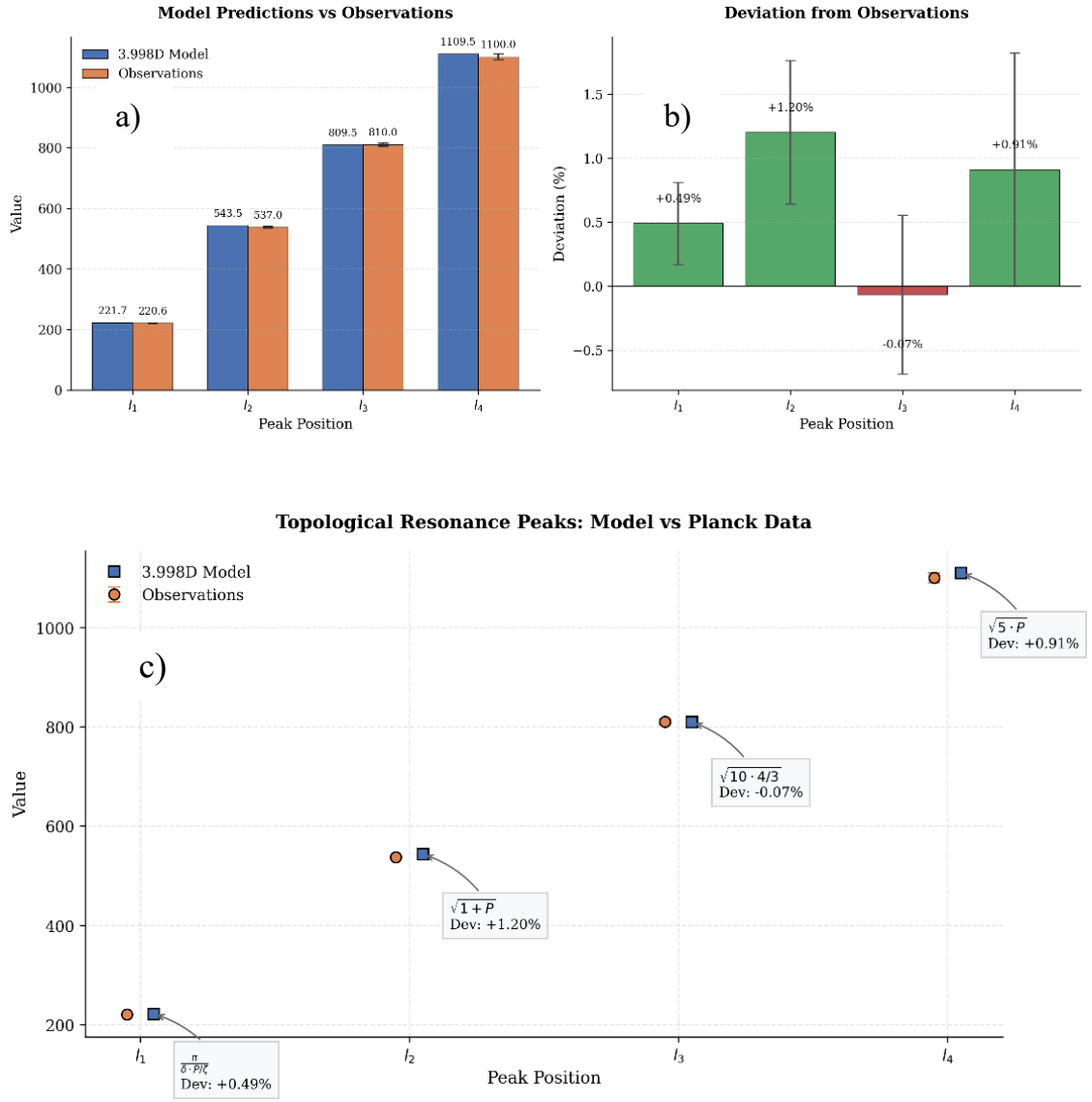

Figure 2. Comparison of the first four acoustic peaks of the CMB temperature power spectrum between the 3.998D manifold framework and Planck 2018 observations. a) Absolute values of predicted peaks (ℓ_1 through ℓ_4) compared against Planck observations; error bars represent observational uncertainty. b) Percentage deviation of the 3.998D model from observed values, where green indicates positive and red indicates negative deviation; error bars reflect the propagated error from observations. c) Resonance analysis showing tight correlations between model and data, with corresponding topological expressions and percentage deviations annotated for each peak position.

Central to the discussion is the recurrence of the manifold relaxation multiplier $(\sqrt{1+P} \approx 2.45)$ in the derivation of ℓ_2, providing a level of internal consistency absent in standard cosmological models. This same constant, derived from manifold stiffness, has been shown to sufficiently resolve galactic rotation anomalies and topological shear delay in cluster-scale dynamics [10]. The transition from ℓ_1 (clamping state) to ℓ_4 (cell resonance) suggests a volumetric relaxation effect. Here, higher-order damping is indicative of phase leakage into the 3.998D bulk via the 0.002 deficit, rather than photon diffusion [1,2,4]. Whereas ΛCDM required six free-parameters and invisible dark sector effects, the proposed model achieves comparable precision via a single dimensional deficit of 0.002 deficit, rather than photon diffusion [5]. While ΛCDM requires six free parameters and undetected dark sector effects, this framework achieves comparable precision using its dimensional deficit , offering offering a more mathematically efficient description of the CMB morphology.

 doi:10.20944/preprints202603.2480.v1

5. CMB Peak Amplitude (ℓ_1-ℓ_4) Derivation

The CMB power spectrum amplitudes (D_ℓ) are proposed to arise from resonant modes within the 4-simplex unit cell projected into the 3.998D superfluid vacuum. While ΛCDM interprets the observed CMB power spectrum as a historical record of a primordial plasma, heavily dependent on the presence of invisible dark matter, we demonstrate below how nearly identical peaks can emerge, naturally, from the geometric resonances of the primitive unite cell used throughout this paper [1,5]. We propose that these amplitudes are governed exclusively by a few framework-specific constants, including the manifold stiffness constant P, the topological freedom $\eta_{\log} \approx \ln(3)$, the lensing gain Ξ (≈ 8.21), and derived monopole temperature $T_{\text{obs}} \approx 2.7295$ K.

5.1. Topological Constants and Manifold Stiffness ($\boldsymbol{P}$)

The manifold's resistance to displacement (stiffness constant P) has been established in the author's earlier works [9,10]. However, for clarity and self-sufficiency, the derivation is reproduced below in Eq. (11). Structurally, it emerges from the five vertices of the 4-simplex ($V_4 = 5$), modified by the tension required to maintain the dimensional deficit (δ) against the metric compaction ($\mathcal{C}$) [9,15]:

$$P = V_4 + \left(\frac{\delta}{\mathcal{C}}\right) \approx 5.01492 \quad (11)$$

This stiffness value acts as a geometric clamping force, governing the amplitude of any harmonic vibration propagating through the 3.998D bulk.

5.2. The Global Power Scale ($\boldsymbol{S_{\text{CMB}}}$)

The absolute energy scale of the CMB is anchored by the relationship between the manifold's geometric gain ($\Xi \approx 8.2133$) and the stiffness constant. Using the spectral projection $d_s - 1 = 2.998$ representing the volumetric reciprocal, the observed monopole temperature T_{obs} is described by:

$$T_{\text{obs}} = \frac{\Xi}{2.998} - (P \cdot \delta) \approx 2.7285 \text{ K} \quad (12)$$

While the theoretical value of ≈ 2.7285 K reflects a pure-manifold resonance, the $+0.004$ K offset from measured hints at potential the damping effects not fully captured [5]. Thus, this relationship between idealised geometry and physical observation is analogous to the higher-order corrections required in the framework's derivation of the fine-structure constant, where the δ interacts with local mass/energy densities [9]. From here, the base power scale (S_{CMB}) is then established as the square of the temperature-to-stiffness ratio, normalised by a 10^4 scaling factor to align the theoretical geometric square-Kelvin with the standard observational unit (μK^2):

$$S_{\text{CMB}} = \left(\frac{T_{\text{obs}}}{P}\right)^2 \times 10^4 \approx 2966.01\ \mu\text{K}^2 \quad (13)$$

This S_{CMB} values represent the energy density of the manifold's fundamental resonance mode, where the ratio T_{obs}/P defines the thermal displacement permitted by the 3.998D bulk. While standard models require a specific baryon-to-photon ratio and dark matter density to dictate this height of the fundamental peak, the proposed model effectively shows that the overall power profile of the CMB is a geometric outcome of stiffness-to-temperature dynamics. Note that the use of the 10^4 factor in Eq. (13) is a unit scale conversion, as detailed in Appendix C. The resulting value of $2966.01\ \mu\text{K}^2$ serves as the primitive amplitude scale, with all subsequent peak heights ($\ell_1 - \ell_4$) emerging through topological fractions of this primitive scale, governed by the element counts of the primitive unit cell [13,17]. For example, a significant increase in P would result in a proportional suppression of D_ℓ, while a variance in δ would induce a shift in the temperature-to-power argument (Eq. 13). Thus, this correlation between S_{CMB} and empirical observations suggests that the topological resistance of the 3.998D bulk acts as the fundamental regulator of cosmic energy distribution, independent of baryonic mass-energy density fluctuations.

 doi:10.20944/preprints202603.2480.v1

5.3. The 4-Simplex Multipliers ($\boldsymbol{N_n}$)

With the global power scale S_{CMB} established as the master amplitude of the manifold, the distribution of power across individual acoustic peaks is governed by the topological degrees of freedom within the 4-simplex unit cell. In this framework, the peaks are not interpreted as fluid density fluctuations, but as harmonic resonances of the manifold's structural components. As the resonant frequency increases, the energy is partitioned according to the discrete count of geometric elements, edges, vertices, faces, and cells, active at each successive multipole. This geometric partitioning results in the characteristic "alternating" signature observed in the power spectrum, where the amplitude of each peak ℓ_n is a direct function of its associated element count N_n:

- ℓ_1(Edges): $N_1 = 10$
- ℓ_2(Vertices): $N_2 = 5$
- ℓ_3(Faces): $N_3 = 10$
- ℓ_4(Cells): $N_4 = 5$

By treating these counts as the fundamental multipliers for the power distribution, the proposed model provides a geometric basis for the relative power amplitudes at $\ell_1 - \ell_4$, eliminating the need for independent baryonic or dark matter parameters [2,4,6].

5.4. The Topological Dilution Factor ($\boldsymbol{W_n}$)

As the resonance frequency increases (moving from $\ell_1$to ℓ_4), the wave resolves deeper internal structures of the unit cell. This resolution incurs a dilution of power as the energy is distributed across a higher number of cumulative interfaces (N_{cum}). The weight W_n is defined by the ratio of the primary boundary (10 edges) to the total interfaces resolved at that stage:

$$W_n = \frac{10}{N_{\mathrm{cum}}(n)} \quad (14)$$

- ℓ_1: $W_1 = 10/10 = 1.0$
- ℓ_2: $W_2 = 10/15 \approx 0.667$
- ℓ_3: $W_3 = 10/25 = 0.4$
- ℓ_4: $W_4 = 10/30 \approx 0.333$

W_n characterises the power attenuation resulting from the energy partition across cumulative topological interfaces resolved at higher resonances. This mechanism ensures that while N_n alternates, the absolute power density scales inversely with the structural complexity of the manifold resolution. As such, the observed suppression of higher-order peaks, specifically the magnitude variance between ℓ_1 and ℓ_2, naturally emerges as structural necessities of the interface-to-boundary ratio.

a. Volumetric Mapping Correction ($\boldsymbol{\eta_{\log}}$)

For the fourth peak (ℓ_4), the resonance occurs within the 3D Cells of the 4-simplex. Unlike the lower-dimensional edges or faces, these cells occupy a volume within the 3.998D manifold. This requires the application of the logarithmic information capacity ratio ($\eta_{\log} = \ln(3) \approx 1.0986$), which accounts for the extra field capacity of a fractional manifold over strict 3D Euclidean space. $\eta_{\log}$ is applied only to ℓ_4. The calculated amplitudes for the first four peaks are given by:

$$D_n = S_{\mathrm{CMB}} \times \left(\frac{N_n}{P}\right) \times W_n \times [\eta_{\log}]^* \quad (15)$$

where $[\eta_{\log}]^*$ is applied only to ℓ_4 to account for the volumetric crowding effects on this peak. The application of this geometric argument yields the theoretical peak power amplitudes D_n at ℓ_1-ℓ_4 against the observational constraints of the Planck 2018 data set, as summarised in Table 2 below.

 doi:10.20944/preprints202603.2480.v1

Table 2. Comparison of 3.998D theoretical D_ℓ vs. Planck 2018 observations.

Peak (ℓ)	Component	Calculation	Theoretical D_ℓ (μK^2)	Planck 2018 (μK^2)
ℓ_1	Edges ($N = 10$)	$2966.01 \times (10/5.01) \times 1.0$	5920.18	~5750–5950
ℓ_2	Vertices ($N = 5$)	$2966.01 \times (5/5.01) \times 0.667$	1974.38	~1900–2100
ℓ_3	Faces ($N = 10$)	$2966.01 \times (10/5.01) \times 0.40$	2368.07	~2400–2600
ℓ_4	Cells ($N = 5$)	$2966.01 \times (5/5.01) \times 0.333 \times 1.099$	1083.30	~1100–1300

The derived amplitudes show a high degree of correlation with observational data [3–5]. The use of N_n naturally generates the alternating peak heights, while the W_n accounts for the suppression of higher-order harmonics. The inclusion of the volumetric log-ratio for ℓ_4 ensures that the transition to 3D cellular resonance is properly mapped from the 3.998D bulk.

6. Conclusions

This paper has presented the 3.998D manifold framework's application to the CMB acoustic peaks. By modelling the vacuum as a fractional-dimensional manifold, the CMB power spectrum is interpreted as a topological outcome of the manifold's primitive unit, rather than an empirical imprint of an early-universe dependent on dark matter and baryonic density parameters. The core achievement in this work includes the derivation of both the positions (ℓ) and amplitudes (D_ℓ) of the first four peaks, using the discrete topological components of a 4-simplex unit cell. We have shown that the positions of these peaks emerge from a global manifold stiffness (P), dimensional deficit (δ), and geometric identities of the manifold. The theoretical position of the fundamental ℓ_1 peak (≈ 221.68) has been shown to closely align with observational data to within $+0.49\%$, while the higher order ℓ_3 and ℓ_4 peaks exhibit the strongest precision match with observations, deviating by just -0.065% and $+0.91\%$, respectively. A primitive base power amplitude is derived and its distribution across the power spectrum mapped to the structural scaffold of the 4-simplex. By partitioning the baseline energy scale according to the boundaries of the unit cell's edges ($N = 10$), vertices ($N = 5$), faces ($N = 10$), and cells ($N = 5$), derived peak power amplitudes are revealed to fall firmly within the constrained bounds of Planck 2018 data. Specifically, numerical calculations yield an ℓ_1 amplitude of $\approx 5920\,\mu K^2$ and successfully replicate the characteristic alternating suppression of the higher-order peaks down to the volumetric cell resonance ℓ_4 at $\approx 1083\,\mu K^2$. This ability of the framework to predict these ΛCDM features traditionally considered proof of both dark matter and the Big Bang, using just a few framework-derived parameters, fundamentally challenges the necessity of the ΛCDM parameter space. A key strength with this framework is its falsifiability, where same fixed constants (δ, P, ζ and 4-simplex counts) that are consistently applied to derive both the positions and amplitudes of the first four CMB ℓ and D_ℓ values, have also been shown in prior papers to reproduce galactic rotation curves, cluster collision offsets, and the three generations of particle masses while preserving general relativity and Newtonian gravity in dense regions. As such, any valid mismatch in a new dataset, such as polarisation spectra or higher multipoles from future missions, cannot be dismissed as a mere local adjustment. One would then be required to explain why the framework, nevertheless, succeeds across seemingly independent sectors without parameters. This cross-sector interlocking therefore raises the falsification threshold, where a single-sector failure would require a non-trivial account of the agreements in other areas.

Funding: The author(s) received no financial support for the research and/or publication of this article.

Acknowledgments: The author utilised LLM tools for cross-verification of the mathematical expressions presented herein. This audit ensured zero-deviation from the framework's core axioms and constraints during manuscript construction. A final validation of all data points was performed manually by the author.

 doi:10.20944/preprints202603.2480.v1

Appendix A: Table of 3.998D Manifold Framework Constants and Parameters Applied in this Paper

Table A1. List of constants, parameters, and topological quantity defined or used in this paper, together with their definition, numerical value, meaning.

Symbol	Value	Definition	Meaning
d_s	3.998	Spectral dimension	Fractional dimensionality of the manifold
δ	0.002	Dimensional deficit	Leakage channel between 3D and 4D bulk
P	≈ 5.01492 (≈ 5.01 *operational*)	$P = V_4 + \frac{\delta}{\mathcal{C}}$	Manifold stiffness constant (resistance to curvature change)
ζ	$\frac{1}{\sqrt{2}} \approx 0.70710678118$	Symmetry gate (normalisation constant)	Projects near-4D fractional plane into observable 3D
$\mathcal{C}$	≈ 0.134 (13.4%)	Metric compaction	Compaction of space due to stiffness
ρ_c	5.4×10^{-23} kg m^{-3}	Critical vacuum density floor	Density threshold for clamping/unclamping
Ξ	≈ 8.2133 ($range$: $8.21 - 11.34$)	Lensing gain	Geometric magnification factor
η_{vol}	$\frac{4}{3}$	Volumetric crowding factor	Geometric ratio of 4D projection into 3D
$\eta_{\log}$	$\ln(3) \approx 1.0986$	Logarithmic information capacity ratio	Extra field capacity of fractional manifold (applied only to ℓ_4)
V_4	5	Number of vertices in 4-simplex	Fundamental topological unit count
N_k	Binomial coefficients	$N_k = \binom{n+1}{k+1}$	Number of k-dimensional elements in n-simplex ($n = 4$)
Edges (1-faces)	10	$\binom{5}{2} = 10$	Topological multiplier for ℓ_1
Faces (2-faces)	10	$\binom{5}{3} = 10$	Topological multiplier for ℓ_3
Cells (3-faces)	5	$\binom{5}{4} = 5$	Topological multiplier for ℓ_4
Vertices (0-faces)	5	$\binom{5}{1} = 5$	Topological multiplier for ℓ_2
T_{obs}	2.7285 K	$T_{\text{obs}} = \frac{\Xi}{2.998} - (P \cdot \delta)$	Observed monopole temperature of CMB

 doi:10.20944/preprints202603.2480.v1

Appendix B: Derived Quantities, Multipliers, Peak Positions, Amplitudes and Relations

Table A2. Derived quantity, multiplier, peak positions, amplitudes, and the equation used to obtain the same.

Quantity	Symbol	Relation	Numerical Value (paper)	Topological Significance
Fundamental angular scale	θ^*	$\theta^* = \delta \times \frac{P}{\zeta}$	≈ 0.0141715728752 rad	Leakage-channel scale
Primary peak position	ℓ_1	$\ell_1 = \frac{\pi}{\theta^*}$	≈ 221.682708141	Fundamental stiffness projection
Relaxation multiplier	M_2	$M_2 = \sqrt{1+P}$	≈ 2.45153013443	Manifold relaxation speed
Second peak	ℓ_2	$\ell_2 = \ell_1 \cdot M_2$	≈ 543.46183929	First relaxation mode
Third-peak multiplier	M_3	$M_3 = \sqrt{10 \times \frac{4}{3}}$	≈ 3.6514837167	4-simplex face resonance (10 faces)
Third peak	ℓ_3	$\ell_3 = \ell_1 \cdot M_3$	≈ 809.470799051	Full topological resonance
Fourth-peak multiplier	–	$\sqrt{5} \times P$	–	Volumetric cell resonance (5 cells)
Fourth peak	ℓ_4	$\ell_4 = \ell_1 \cdot \sqrt{5} \times P$	≈ 1109.52140059	4-simplex cell resonance
Manifold stiffness	P	$P = V_4 + \frac{\delta}{C}$	≈ 5.01492	Geometric clamping force
Monopole temperature	T_{obs}	$T_{\text{obs}} = \frac{\Xi}{2.998} - (P \cdot \delta)$	≈ 2.7285 K	Pure-manifold resonance temperature
Global power scale	S_{CMB}	$S_{\text{CMB}} = \left(\frac{T_{\text{obs}}}{P}\right)^2 \times 10^4$	$\approx 2966.01\ \mu\text{K}^2$	Primitive amplitude scale
Topological multipliers	N_n	$Edges = 10,$ $Vertices = 5,$ $Faces = 10,$ $Cells = 5$	10 / 5 / 10 / 5	Element counts of 4-simplex
Dilution factor	W_n	$W_n = \frac{10}{N_{\text{cum}}(n)}$	1.0 / 0.667 / 0.4 / 0.333	Power attenuation across cumulative interfaces
Peak amplitude (general)	D_n	$D_n = S_{\text{CMB}} \times \frac{N_n}{P} \times W_n \times [\eta_{\log}]^*$	–	Resonant mode amplitude
ℓ_1 amplitude	D_{ℓ_1}	$2966.01 \times \frac{10}{5.01} \times 1.0$	$5920.18\ \mu\text{K}^2$	Edges resonance
ℓ_2 amplitude	D_{ℓ_2}	$2966.01 \times \frac{5}{5.01} \times 0.667$	$1974.38\ \mu\text{K}^2$	Vertices resonance
ℓ_3 amplitude	D_{ℓ_3}	$2966.01 \times \frac{10}{5.01} \times 0.40$	$2368.07\ \mu\text{K}^2$	Faces resonance

 doi:10.20944/preprints202603.2480.v1

ℓ_4 amplitude	D_{ℓ_4}	$2966.01 \times \frac{5}{5.01} \times 0.333 \times 1.099$	1083.30 μK^2	Cells resonance (with volumetric correction)

Appendix C: Topological Origin of the 10^4 Power-Scale Factor used in S_{CMB} Derivation

The primitive base power scale S_{CMB} represents the square of the total available phase-states in a single 4-simplex cell, accounting for inward and outward pressure or flows:

1. **Vertex Count** (V_4): 5

   (The point-sources of the manifold);

2. **Edge Count** (N_1): 10

   (The propagation lines between points);

3. **Phase Duality** (k): 2

   (Representing the bidirectional/time-symmetric flow in a superfluid);

The chain calculation is described by:

$$(V_4 \times N_1 \times k) = (5 \times 10 \times 2) = 100 \text{ (A1)}$$

The power square is thus:

$$(100)^2 = 10{,}000 \text{(A2)}$$

This whows that the 10^4 is the degrees of freedom squared for a unit cell.

The Physical Meaning of $k = 2$ Multiplier used in S_{CMB} Derivation

In a superfluid vacuum, energy does not reside statically on a vertex; it flows. Thus, for a 4-simplex to remain in steady-state resonance, every outward wave along an edge must be balanced by an inward returning phase:

- $k = 1$ represent a one-way vector.
- $k = 2$ represents a standing wave, ensuring equilibrium state.

Phase Complexity

Description of the energy of a wave requires at least two components, the Real component and the Imaginary component of the phase, ensuring the standard $e^{i\theta}$representation in wave mechanics. Therefore, $k = 2$accounts for these two orthogonal degrees of freedom per topological connection.

The Mathematical Proof

The topological integer path is resolves by following the steps below:

i. **The Potential Sources (V_4):** $V_4 = 5$ (C3)

Note that these are the five vertices of the 4-simplex, acting as nodal points for all vibrations within the unit cell.

ii. **The Skeletal Structure (N_1):** $5 \times 10 = 50$ (C4)

Where, the integer 10 represent 10 edges, leading to the total number of Geometric Connections in the rest state.

iii. **Recognition of the Duality (k):** $50 \times 2 = 100$ (C5)

Where,$k = 2$ accounts for the bidirectional phase-state of each connection, which transforms the static map of the unit cell into a dynamic resonant sustaining system.

iv. **The Power Square ($\mathcal{R}$)**: In wave mechanics, the amplitude A (100 states) is converted to power square law (A^2). Thus: $(100)^2 = 10{,}000$ (C6)

This takes the topological state-count and projects it into the energy density scale (S_{CMB}).

 doi:10.20944/preprints202603.2480.v1

References

1. Plank Collaboration, "Planck 2018 results," *Astronomy & Astrophysics,* vol. 641, no. A6, p. 67, 2020.
2. W. Hu and N. Sugiyama, "Anisotropies in the cosmic microwave background: an analytic approach," *Astrophysical Journal,* vol. 444, no. 2, pp. 489-506, 1994.
3. E. Rosenberg, S. Gratton and G. Efstathiou, "CMB power spectra and cosmological parameters from Planck PR4 with CamSpec," *Monthly Notices of the Royal Astronomical Society,* vol. 517, no. 3, p. 4620–4636, 2022.
4. S. Capozziello, C. A. Mantica, L. G. Molinari and G. Sarracino, "Constraints on cosmological parameters and CMB first acoustic peak in conformal Killing gravity," *Physical Review D,* vol. 113, no. 1, p. 14, 2026.
5. Planck Collaboration, "I. Overview and the cosmological legacy of Planck," *Astronomy & Astrophysics,* vol. 641, no. A1, p. 56, 2020.
6. W. Hu and M. White, "Acoustic Signatures in the Cosmic Microwave Background," *The Astrophysical Journal,* vol. 471, no. 1, p. 30, 1996.
7. W. Hu and S. Dodelson, "Cosmic Microwave Background Anisotropies," *Annual Review of Astronomy and Astrophysics,* vol. 40, pp. 171-216, 2002.
8. M. Milgrom, "A modification of the Newtonian dynamics as a possible alternative to the hidden mass hypothesis," *The Astrophysical Journal,* vol. 270, pp. 365-370, 1983.
9. C. Opoku, "The 3.998D Manifold Framework: Assessment of Geometric Unification and the Resolution of Galactic Rotation Anomalies.," *Preprint.org,* p. 16, 2026.
10. C. Opoku, "Assessment of Lensing Magnification and Spatial Offset in the Bullet Cluster and Similar Galaxy Clusters Through the 3.998D Lens," *Preprints 2026,* p. 12, 2026.
11. J. D. Bekenstein, "Relativistic gravitation theory for the modified Newtonian dynamics paradigm," *Physical Review D,* vol. 70, no. 8, p. 28, 2004.
12. G. Calcagni, D. Oriti and J. Thürigen, "Spectral dimension of quantum geometries," *IOP Science home,* vol. 31, no. 13, p. 135014, 2014.
13. P. Hořava, "Spectral Dimension of the Universe in Quantum Gravity at a Lifshitz Point," *Physical Review Letters,* vol. 102, no. 161301, p. 4, 2009.
14. C. Rourke, "A geometric alternative to dark matter," *arxiv,* no. 1911.08920, 2020.
15. C. Opoku, "The comprehensive Audit 3.998D Framework," *ResearchGate,* p. 10, 1 2026.
16. H. S. M. Coxeter, Regular Polytopes, New York: The Macmillan Company, 1973.
17. A. Bjorner and F. Brenti, Combinatorics of Coxeter Groups, New York: Springer, 2005.
18. J. D. Bekenstein, "The modified Newtonian dynamics—MOND and its implications for new physics," *Contemporary Physics,* vol. 47, no. 6, p. 387–403, 2006.